The Barcelona-Catania-Paris-Madrid Energy Density Functional and Its Application to the EOS of Neutron Stars

X. Viñas[1], **M. Baldo**[2], **G.F. Burgio**[2] **M. Centelles**[1],
L.M. Robledo[3], **B.K. Sharma**[1,4]

[1]Departament d'Estructura i Constituents de la Matèria and Institut de Ciències del Cosmos, Universitat de Barcelona, E-08028 Barcelona, Spain

[2]INFN Sezione di Catania, I-95123 Catania, Italy

[3]Departamento de Física Teórica, Universidad Autónoma de Madrid, E-28049 Madrid, Spain

[4]Department of Sciences, Amrita University, 641112 Coimbatore, India

Abstract. We present the most recent version of the Barcelona-Catania-Paris-Madrid energy density functional which is largely based on *ab initio* calculated symmetric and neutron matter equations of state. This functional contains two free parameters related to the nuclear matter and surface energies. An *rms* deviation of 1.58 MeV is obtained from the fit of these parameters to 579 measured nuclear masses. This deviation compares favourably with the one obtained using other mean field theories. This functional is applied to describe the structure of Neutron Stars from the outer crust to the core. Comparison with other Neutron Star equations of state are discussed. The relevance of the crust equation of state for the Neutron Star radius is pointed out.

1 Introduction

The physics of atomic nuclei and nuclear systems is very rich but extremely complicated to describe. In principle one should start from the bare nucleon-nucleon interaction which is well determined at long distances although at short distances the repulsive core is less known. The short-range in-medium correlations (Pauli blocking) cancel out the repulsive core and yield a smooth in medium interaction. Handling of the short range correlations require Brueckner like methods which are extremely hard to implement in finite nuclei. Therefore, the smooth effective interaction is replaced by effective interactions like the Skyrme and Gogny forces or the Relativistic Mean Field (RMF) model.

The non-relativistic zero-range Skyrme [1] and finite-range Gogny [2] forces consist of the central, Coulomb and spin-orbit contributions plus a phenomenological density-dependent term. In the relativistic models it is assumed that baryons interact by exchanging scalar and vector mesons and are described through a relativistic Lagrangian [3]. There are several hundreds of Skyrme and RMF interactions of different type whose parameters are usually fitted to

reproduce a few nuclear matter properties and the ground state of a reduced set of finite nuclei. Most of these interactions are taylored to describe specific problems. Although many of such parametrizations give a more or less reasonable description of stable nuclei, they predict divergent results when extrapolated to regions where there is not experimental data. To cure these deficiencies, modern parametrizations introduce more information from symmetric and neutron matter in order to constrain their parameters. On the other hand, the binding energy of all the nuclei experimentally known are used as input to fit the parameters of the interaction. Skyrme SLy, SV, UNEDFX, HFB-21 and Gogny D1N and D1M are examples of these modern effective interactions.

In a set of recent papers [4–6] we have presented a new energy density functional (EDF) called BCPM (Barcelona-Catania-Paris-Madrid) aimed to describe ground-state binding energies of finite nuclei with a quality similar to the one provided by successful Skyrme and Gogny forces. Inspired by the Kohn-Sham (KS) theory, instead of starting from an effective interaction, we directly construct an EDF that contains a bulk part obtained from *ab initio* microscopic calculations of Brueckner-Hartree-Fock (BHF) type in symmetric and neutron matter, and a phenomenological surface part together with the Coulomb and spin-orbit contributions. This BCPM EDF contains eventually only two open parameters which are fitted to reproduce the experimental binding energy of 579 spherical and deformed even-even nuclei.

We use this microscopically based BCPM EDF to describe the structure of neutron stars (NS) from the outer crust to the core and compare with few other EOS that encompass the whole NS structure. In particular we compare our results with the predictions of the EOSs of Lattimer and Swesty (LS) [7], Shen [8] and Douchin and Haensel [9]. More recently, other EOSs covering the whole NS have been derived by the Brussels-Montreal group [10] using the modern Skyrme forces BSk19, BSk20 and BSk21 [11]. Some first results about the BCPM EOS have been reported recently [12].

The paper is organized as follows. In the first section we briefly revise the BCPM EDF. The second section is devoted to the description of the crust of NS. In the third section we discuss the liquid core and the mass-radius relationship. Finally our conclusions are presented in the last section.

2 The BCPM Energy Density Functional

The BCPM EDF is based on the Kohn-Sham density functional theory (KS-DFT) where the one-body density $\rho(\mathbf{r})$ plays a central role. In this theory one introduces an auxiliary set of A orthonormal orbitals $\phi_i(\mathbf{r}, \sigma, \mathbf{q})$, where A is the nucleon number and σ and q the spin and isospin indices, respectively, which allows to express the one-body density as a Slater determinant build up with the orbitals ϕ_i, i.e $\rho(\mathbf{r}) = \sum_{\mathbf{i},\sigma,\mathbf{q}} |\phi_{\mathbf{i}}(\mathbf{r}, \sigma, \mathbf{q})|^2$. Within the KS-DFT the energy splits into two parts $E = T_0[\rho] + W[\rho]$. The uncorrelated kinetic energy T_0 is written in terms of the orbitals as $T_0 = (\hbar^2/2m) \sum_{i,\sigma,q} |\nabla\phi_i(\mathbf{r}, \sigma, \mathbf{q})|^2$. The

interacting part $W[\rho]$ contains the potential energy and the correlated part of the kinetic energy. The potential energy is given by the sum of the nuclear, Coulomb and spin-orbit contributions:

$$E = T_0 + E_N + E_{Coul} + E_{s-o}. \tag{1}$$

The nuclear potential energy is divided into a bulk part and a surface contribution, i.e. $E_N = E_N^{bulk} + E_N^{surf}$. The bulk part is obtained from the interaction energy term of the microscopic EOS in symmetric and neutron matter. These EOSs are calculated in good accuracy in the Brueckner two hole lines approach with the continuous choice for the single-particle potential [13]. In the BHF approximation the energy per particle reads:

$$\frac{E}{A} = \frac{3}{5}\frac{\hbar^2 k_F^2}{2m} + \frac{1}{2\rho}\sum_{k,k'<k_F} \left\langle kk' \middle| G[\rho; e(k) + e(k')] \middle| kk' \right\rangle_a, \tag{2}$$

where $G(\rho, \omega)$ is the Brueckner reaction matrix solution of the Bethe-Goldstone equation

$$G[\rho; \omega] = V + \sum_{k_a,k_b} V \frac{|k_a k_b > Q < k_a k_b|}{\omega - e(k_a) - e(k_b)} G[\rho; \omega]. \tag{3}$$

In (2) V is the bare nucleon-nucleon interaction, ρ – the number density,

$$e(k) = \frac{\hbar^2 k^2}{2m} + U(k,\rho) \tag{4}$$

is the single-particle energy and Q is the Pauli operator that determines the propagation of intermediate baryon pairs. The single-particle potential $U(k,\rho)$ using the continuous choice reads

$$U(k;\rho) = \text{Re} \sum_{k'<k_F} \left\langle kk' \middle| G[\rho; e(k) + e(k')] \middle| kk' \right\rangle_a, \tag{5}$$

In (2) and (5) the subscript "a" indicates antisymmetrized matrix elements. Eqs.(2)-(5) constitute a coupled system of equations that has to be solved self-consistently. Once the G matrix is known, the energy per particle is easily computed with (1).

This BHF calculation has been performed using the Argonne v_{18} potential as two-nucleon interaction. To reproduce the correct saturation point in symmetric nuclear matter, three-body forces based on the so-called Urbana model have to be added (see [6] and [12] for details). These EOSs are compatible with phenomenological constraints from heavy-ion reactions as well from the analysis of astrophysical observations [14].

The bulk part of the BCPM EDF for finite nuclei stems directly from these microscopic EOSs in the spirit of the LDA (Local Density Approximation). For computational purposes, an educated fifth degree polynomial fit as a function of

X. Viñas, M. Baldo, G.F. Burgio, M. Centelles, L.M. Robledo, B.K. Sharma

the total density is performed on top of the microscopic calculation constrained to have the saturation point at E/A=-16 MeV at a density ρ_0=0.16 fm^{-3}. The fitting polynomials $P_s(\rho)$ and $P_n(\rho)$ for symmetric and for neutron matter, respectively are given in Table 1 of [6].

The bulk energy contribution to the EDF is obtained by a quadratic interpolation between $P_s(\rho)$ and $P_n(\rho)$ in terms of the asymmetry parameter $\beta = (\rho_n - \rho_p)/\rho$ between the symmetric and neutron EOS:

$$E_N^{bulk}[\rho_p, \rho_n] = \int d\vec{r}\big[P_s(\rho)(1 - \beta^2) + P_n(\rho)\beta^2\big]\rho \qquad (6)$$

The surface contribution to the interacting nuclear energy is written as:

$$E_N^{surf}[\rho_n, \rho_p] = \frac{1}{2}\sum_{t,t'}\iint d\vec{r}d\vec{r'}\rho_t(\vec{r})v_{t,t'}(\vec{r} - \vec{r'})\rho_{t'}(\vec{r'}) \qquad (7)$$

where the index t is the label for neutron and protons and $v_{t,t} = V_{t,t}e^{-r^2/r_{0tt}^2}$ is the finite range form factor of Gaussian type. The strengths $V_L(t = t')$ and $V_U(t \neq t')$ have been determined in such a way that in the uniform density limit of (7) reproduces the ρ^2 term of the bulk part (6). This implies that $V_{nn} = V_{pp} = \frac{2\bar{b}_1}{\pi^{3/2}r_{0L}^3\rho_0}$ and $V_{np} = V_{pn} = \frac{4a_1-2\bar{b}_1}{\pi^{3/2}r_{0U}^3\rho_0}$, where $\bar{b}_1 = b_1\rho_0/\rho_{0n}$, being a_1 and b_1 the coefficients of the ρ^2 of the polynomials $P_n(\rho)$ and $P_n(\rho)$, respectively. Therefore, the ranges r_{0L} and r_{0U} are the free parameters to be fitted using finite nuclei data.

The Coulomb term in (1) contains the standard direct and the Slater contributions calculated from the proton density. The spin-orbit term in (1) has the same form as in the Skyrme and Gogny interactions with a strength W_0 that is also an open parameter. The finite nuclei calculations are performed in the mean-field approximation using the Hartree-Fock-Bogoliubov (HFB) approximation. The pairing interaction is a zero-range density dependent force adjusted to reproduce the neutron gap predicted by the Gogny force in symmetric nuclear matter with $m^* = m$ [15]. We also include in our calculation the two-body center of mass correction using a pocket formula based on the harmonic oscillator [16]. These HFB calculations in finite nuclei are restricted to axially symmetric solutions computed in a harmonic oscillator basis using an approximated second-order gradient method. The calculated binding energy is the HFB one supplemented with the rotational energy correction and an estimate of the finite size of the basis (see [6] for details).

The three initial parameters, i.e. the ranges r_{0L}, r_{0U} and the strength of the spin-orbit interaction W_0, are fitted to minimize the *rms* deviation for the binding energies: $\sigma(E)^2 = \sum_1^N[B_{th}(i) - B_{exp}(i)]^2/N$ where the sum runs over a set of 579 even-even nuclei with known binding energies [17]. From these fits it is found that $\sigma(E)$ has a very smooth dependence on W_0 and its minimal value is always around 90 MeV fm^5. Another relevant information is that
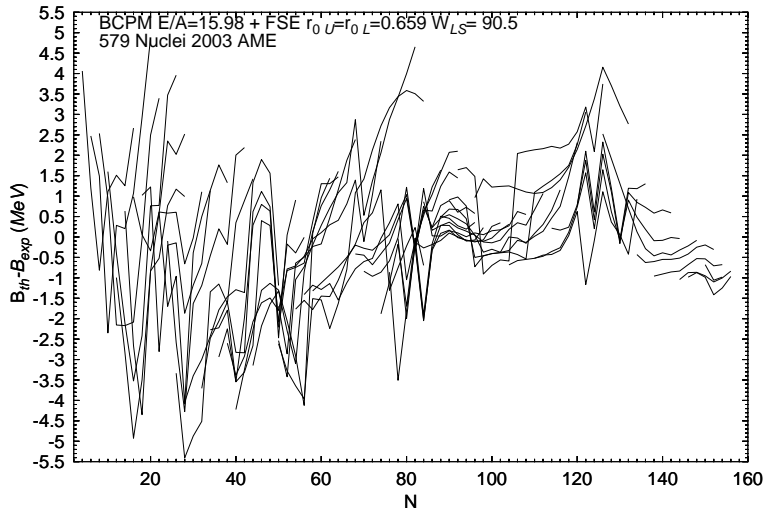
Figure 1. Binding energy differences as a function of the neutron number predicted by the BCPM EDF.

$\Delta B = B_{th} - B_{exp}$ shows a linear dependence on A and its slope depends on the energy per particle E/A at the minimum of the polynomial fit of the symmetric nuclear matter $P_s(\rho)$. It is found that E/A=-15.98 MeV yields the lowest $\sigma(E)$ value and almost zero slope. It is also found that the minimal value of $\sigma(E)$ is achieved for $r_{0L} = r_{0U} \simeq 0.66$ fm. After all these considerations we conclude that E/A=-15.98 MeV, W_0=90.5 MeV fm^5 and $r_{0L} = r_{0U}$=0.659 fm is the best choice for the open parameters of BCPM EDF giving $\sigma(E)$=1.58 MeV. The differences ΔB computed with these optimal parameters are displayed in Figure 1. We have also computed the charge radii using a proton radius of 0.875 fm. The rms value $\sigma(R)$ obtained using 313 experimental values of even-even nuclei [18] is 0.027 fm.

We compare our results with those obtained using different parametrizations of the Gogny force. The $\sigma(E)$ and $\sigma(R)$ values obtained in the same conditions using the D1S and D1M Gogny forces are 2.13 MeV and 0.037 fm and 1.47 MeV and 0.028 fm, respectively. The analysis of the quadrupole and octupole deformations in the ground-state and fission barriers [19] reveal that the predictions of the BCPM EDF are quite similar to the ones of the D1S and D1M forces. Comparisons of the BCPM EDF calculations with the results provided by modern Skyrme interactions shows that the energy *rms* for a similar number of nuclei is also similar to the one obtained with the BCPM EDF. Only the HFB-21 parametrization obtained by the Brussels group [11] exhibit a $\sigma(E)$ value of 0.58 MeV. However HFB-21 include a larger set of odd and even nuclei (2149) and also the model includes some phenomenological aspects not considered in the BCPM EDF.

3 The Crust of the Neutron Stars

Now we use the BCPM EDF to compute the EOS of nonaccreting cold NS from the solid outer core to the liquid core of the star. To use the same EDF for the whole structure of the star allows to obtain a consistent and unified description which stems from underlying microscopic grounds. We will discuss this BCPM EOS and will perform comparisons with other available EOS devised to cover the whole structure of the NS. It is assumed that the crust of a NS has the structure of regular lattice which is treated in the Wigner-Seitz (WS) approximation where the unit cell, with a cubic or more complicated structures, is replaced by a spherical cell with the same volume.

3.1 The outer crust

The outer crust of a NS is composed by neutron rich nuclei and free electrons at densities approximately between 10^4 and 4×10^{11} g/cm^3 above which the neutrons start to drip from the nuclei. The outer crust is fully ionized and the atomic nuclei arrange themselves in a body-centered cubic lattice in order to minimize the Coulomb repulsion among them. Nuclei are stabilized against β decay by the surrounding electron gas. At very low densities around 10^4 g/cm^3, the lattice is populated by ^{56}Fe nuclei and the effect of the electrons is negligible. When the average baryon density increases, the importance of the electrons increases too, and becomes energetically favourable for the system to reduce the proton ratio by electron captures with the energy carried away by neutrinos. Consequently, the system evolves towards a Coulomb lattice of more and more neutron rich nuclei until the neutron drip density is reached and the inner crust of NS begins.

The outer crust of NS is studied following the well known formalism of Baym, Pethick and Sutherland [20]. In this model the energy density at a given density is given by the sum of the nuclear, electronic and lattice parts, i.e. $\mathcal{E}(A, Z, \rho_B) = \mathcal{E}_n + \mathcal{E}_{elec} + \mathcal{E}_l$. The nuclear contribution is the nuclear energy per nucleon that is obtained using the BCPM EDF described in the previous Section. The electronic part is provided by the relativistic free Fermi gas of electrons which reads:

$$\mathcal{E}_{elec} = \frac{m_e^4}{8\pi^2} \left[x_e \left(2x_e^2 + 1 \right) \sqrt{x_e^2 + 1} - \ln \left(x_e + \sqrt{x_e^2 + 1} \right) \right], \qquad (8)$$

with $x_e = p_F^e / m_e$, being p_F^e the electron Fermi momentum and m_e its mass. The lattice contribution corresponding to the interaction between protons located in the lattice and free electrons is approximated by a Coulomb mass formula-like term [21].

The minimization of the energy per baryon at given baryonic density allows to obtain the optimal nuclear composition (A, Z) as well as the pressure corresponding at such a density, i.e. the EOS of the outer crust. Notice that only the electronic and lattice terms contribute to the pressure in the outer crust, i.e.
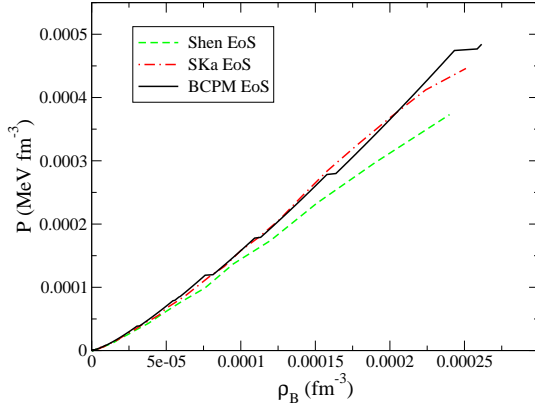
Figure 2. EOS corresponding to the outer crust of a Neutron Star computed with different models.

$P = P_{elect} + P_l$. The BCPM EOS corresponding to the outer crust is displayed in Figure 2, and compared with the predictions of the Lattimer-Swesty (LS) and Shen models that are devised to describe the whole EOS. The BCPM EOS agrees well with the LS EOS and both of them show some discrepacies with the Shen EOS in this range of densities. From this Figure we see that the BCPM EOS shows small jumps in the average density for some values of the pressure. These jumps appear when the equilibrium nucleus change to another varying its composition (A, Z). These jumps are absent in the LS and Shen EOS because they are of semiclassical type and (A, Z) vary in a continuous way in this case. The BCPM EOS in the outer crust lies close to the LS and Shen predictions. This result seems to point out that in the outer crust shell effects may be not very relevant to calculate the pressure although they are essential to estimate the composition of the most stable nucleus as a function of the average density.

3.2 The inner crust

In our model the inner crust EOS is obtained by means of a self-consistent Thomas-Fermi (TF) calculation. There are two comments about the choice of this method. On the one hand, it is expected, as it happens in the outer crust calculations, that shell effects, neglected in the TF approach, have little impact on the EOS. On the other hand, TF calcuations can easily be performed using not only spherical WS but also cells with different geometries allowing to study different pasta phases. The total energy of an ensemble of neutron, proton and electrons in a WS cell of volume V_c is given by

$$E = \int dV \left[\mathcal{H}(\rho_n, \rho_p) + \mathcal{E}_{elec} + \mathcal{E}_{coul} \right.$$
$$\left. - \frac{3}{4}\left(\frac{3}{\pi}\right)^{1/3} e^2 \left(\rho_p^{4/3} + \rho_e^{4/3}\right) + m_n \rho_n + m_p \rho_p \right], \quad (9)$$

59

where the nuclear energy density in the TF approach reads

$$\mathcal{H}\left(\rho_n,\rho_p\right)=\frac{\hbar^2}{2m_n}\frac{3}{5}\left(3\pi^2\right)^{2/3}\rho_n^{5/3}+\frac{\hbar^2}{2m_p}\frac{3}{5}\left(3\pi^2\right)^{2/3}\rho_p^{5/3}+\mathcal{V}\left(\rho_n,\rho_p\right) \quad (10)$$

and the Coulomb direct energy is given by

$$
\begin{aligned}
\mathcal{E}_{coul} &= \frac{1}{2}\left(\rho_p(\mathbf{r})-\rho_e\right)\left(V_p(\mathbf{r})-V_e(\mathbf{r})\right) \\
&= \frac{1}{2}\left(\rho_p(\mathbf{r})-\rho_e\right)\int\frac{e^2}{|\mathbf{r}-\mathbf{r'}|}\left(\rho_p(\mathbf{r'})-\rho_e\right)d\mathbf{r'}.
\end{aligned}
\quad (11)
$$

where it is assumed that the electrons are uniformly distributed in the cell. The non-interacting part of the electrons $\mathcal{E}_{elec}$ is given again by (8).

We perform a fully self-consistent calculation of the energy in a WS cell of fixed radius R_c under the constraints of given average density ρ_B and charge neutrality. Taking functional derivatives in (9) with respect to the neutron, proton and electron densities, one finds a set of coupled integral equations for these densities together with the β equilibrium condition $\mu_e=m_n+m_p+\mu_n-\mu_p$ (see [12] for more details).

By solving such a system one finds the composition (A,Z) of minimal energy corresponding to the prescribed ρ_B and R_c satisfying β-equilibrium. Next, a search of the optimal size of the cell is performed by repeating the calculation for different values of the radius R_c with the same average density ρ_B. This calculation is very delicate from the numerical point of view. The reason is that the minimal energy as a function of R_c is usually extremely flat and the differences of the total energies involved are of the order of a fraction of few keV and sometimes only of some eV. The self-consistent TF calculation described here can be extended to WS cells with planar (slabs) and cylindrical (rods), and also allows to compute spherical and cylindrical bubbles. These calculations with non-spherical symmetry are simplified if one considers slabs or rods of infinite extension in the perpendicular direction to R_c. Although in the cases of non-spherical geometries the total number of particles and the energy are infinite, the number of particle and the energy per unit of surface (slabs) or per unit of length are finite. At densities close to the transition to the core, the differences of energies computed in WS cells with different geometries is usually very small and a careful numerical analysis must be performed to determine the configuration with minimal energy. For example at a density $\rho_B=0.077$ fm^{-3}, the optimal configuration corresponds to a WS cell with cylindrical symmetry which differ from the spherical solution by only 527 eV.

Once the energy is computed, the pressure in the inner crust WS cell can be obtained by taking the derivative of the energy with respect to the size of the cell [22]. The resulting pressure is: $P=P_g+P_{elect}+P_{ex}$, which shows that the pressure in the inner crust is due to the sum of the contributions of the neutron gas and free electrons plus a corrective term coming from the electron
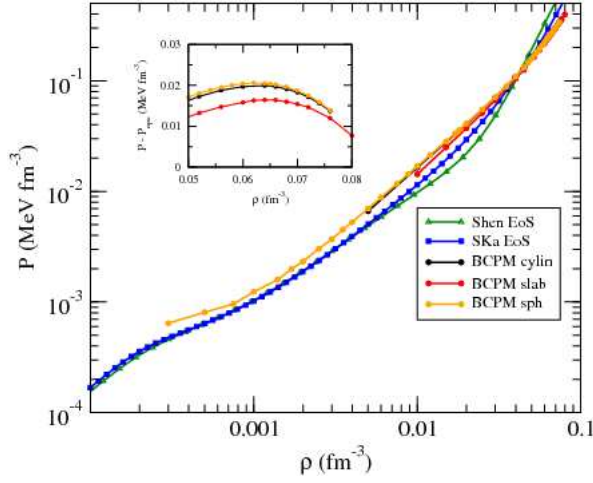
Figure 3. EOS corresponding to the inner crust of a Neutron Star computed with different models. The inset corresponds to the BCPM EDF pressure obtained with different geometries.

exchange. In Figure 3 we compare the BCPM EOS in the inner crust with the predictions of the LS and Shen models. We see that the pressures computed with BCPM show some differences with the values predicted by the LS and Shen calculations. From the same Figure we can also see that in the BCPM EOS the spherical structure practically dominates the whole inner crust. Only at high densities close to the transition density to the core, pasta phases are the most favourable configuration because these phases provide the highest pressure.

4 The Liquid Core and the Mass Radius Relationship

The liquid core a of NS consists of a uniform mixture of neutron, protons and leptons (e^-, μ^-) in beta equilibrium. Therefore the energy density in this region can be written as

$$
\mathcal{E}(\rho_n, \rho_p, \rho_e, \rho_\mu) = (\rho_n m_n + \rho_p m_p) + (\rho_n + \rho_p)\frac{E}{A}(\rho_n, \rho_p)
$$
$$
+ \rho_\mu m_\mu + \frac{\hbar^2}{2m_\mu}\frac{(3\pi^2\rho_\mu)^{5/3}}{5\pi^2} + \frac{\hbar(3\pi^2\rho_e)^{4/3}}{4\pi^2} , \quad (12)
$$

where we have considered ultrarelativistic electrons and relativistic muons. The energy per particle in asymmetric nuclear matter is well estimated by a quadratic interpolation in terms of the asymmetry β between the EOS of symmetric and neutron matter as we have discussed in Section 1. The chemical potential of the different species is computed straightforwardly as $\mu_i = \partial\varepsilon/\partial\rho_i (i = n, p, e, \mu)$. The beta equilibrium condition $\mu_i = b_i\mu_n - q_i\mu_e$ (where b_i and q_i denote

61

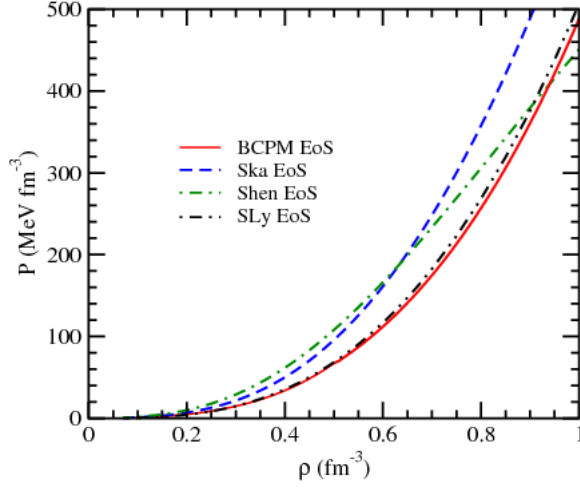*X. Viñas, M. Baldo, G.F. Burgio, M. Centelles, L.M. Robledo, B.K. Sharma*

Figure 4. EOS corresponding to beta-stable matter computed with different models.

the baryon number and the charge of the species i) and the charge neutrality $\sum_i \rho_i q_i = 0$ allow to determine the equilibrium composition $\rho_i(\rho)$ at given baryon density ρ. Finally the EOS of the core reads:

$$P(\rho) = \rho^2 \frac{d}{d\rho} \frac{\mathcal{E}(\rho_i(\rho))}{\rho} = \rho \frac{d\mathcal{E}}{d\rho} - \mathcal{E} = \rho \mu_n - \mathcal{E} \qquad (13)$$

The BCPM EOS is displayed in Figure 4 from the outer crust to the core up to a density ρ=1 fm^{-3} together with the predictions of the LS (label Ska), Shen and Douchin-Haensel (label SLy) EOS. We notice a remarkable similarity between the BCPM EOS and the one of Douchin-Haensel based on the Skyrme force SLy4 and a strong difference with the LS and Shen EOS which are stiffer than the BCPM EOS.

Once the full EOS from the outer crust to the core is known, the relation between the mass and radius of a NS can be obtained using the well known Tolman-Oppenheimer-Volkov equation (see [12] for details). The mass-radius relationships computed with the BCPM, LS and Shen EOSs are displayed in Figure 5. The mass of the NS as a function of the radius has a maximum value above which the star is unstable against collapse to a black hole. The EOS displayed in Figure 5 are compatible with the largest mass observed up to now which is $2.01 M_\odot \pm 0.04$ [23]. From Figure 5 one can also see the influence of the crust in the mass-radius relationship. In addition to the full BCPM calculation, we also display the mass-radius relationship computed with the BCPM EOS in the core but using for the crust the EOS provided by Shen (squares) and LS (circles). The effect of the EOS of the crust on the size of the star is relevant for NS masses smaller than 1.2-1.3 solar masses pointing out the importance of
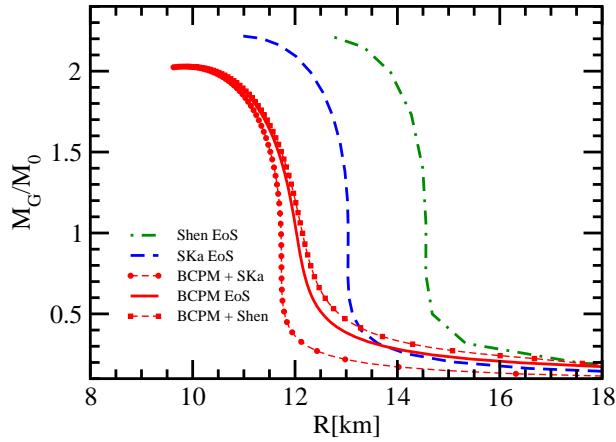
Figure 5. Neutron Star gravitational mass as a function of the radius (see the text for details).

using an EOS derived from same theoretical scheme to investigate the structure of the NS.

5 Conclusions

In the first part of this work we have revised the energy density functional BCPM based on a fit to realistic EOS in symmetric and neutron matter, and applied to finite nuclei through LDA. This functional contains essentially two free parameters to be adjusted from finite nuclei data. Due to its local character, calculations of finite nuclei are very fast. The quality of binding energies and charge radii predicted by the BCPM energy density functional are comparable to those computed with modern versions of Gogny and Skyrme forces. The deformation properties of nuclei obtained using the BCPM energy density functional are similar to those predicted by the D1S Gogny force.

In the second part of the work we have studied the structure of the neutron stars from the outer crust to the core using the BCPM energy density functional. This is an attempt to describe the whole structure of NS using a model based on microscopic grounds. The composition and EOS of the outer crust is obtained from masses computed with the HFB method. The EOS in the inner crust is obtained by means of a self-consistent Thomas-Fermi approximation which also allows to investigate pasta phases.The structure of the neutron stars predicted by the BCPM energy density functional has been compared with the results provided by other more phenomenological EOS. The analysis of the mass-radius relationship in NS shows that the EOS in the crust has sizeable effects on the radius of the star pointing out the importance of using models based on the same physical framework for both crust and core.

X. Viñas, M. Baldo, G.F. Burgio, M. Centelles, L.M. Robledo, B.K. Sharma

References

[1] E. Chabanat, P. Bonche, P. Haensel, J. Meyer and R. Schaeffer, *Nuc. Phys. A* **635** (1998) 441.

[2] J. Dechargé and D. Gogny, *Phys. Rev. C* **21** (1996) 1568.

[3] B.D. Serot and J.D. Walecka, *Adv. Nucl. Phys.* **16** (1986) 1.

[4] M. Baldo, P. Schuck and X. Viñas, *Phys. Lett. B* **663** (2008) 390.

[5] M. Baldo, L.M. Robledo, P. Schuck and X. Viñas, *J. Phys. G: Nucl. Part. Phys.* **37** (2010) 064015.

[6] M. Baldo, L.M. Robledo, P. Schuck and X. Viñas, *Phys. Rev. C* **87** (2013) 064305.

[7] J.M. Lattimer and F.D. Swesty, *Nuc. Phys. A* **535** (1991) 331.

[8] H. Shen, H. Toki, K. Oyamatsu and K. Sumiyoshi, *Prog. Theor. Phys.* **100** (1998) 1013; *Nuc. Phys. A* **637** (1998) 435.

[9] F. Douchin and P. Haensel, *Astron. Astrophys.* **389** (2001) 151.

[10] A.F. Fantina, N. Chamel, J.M. Pearson and S. Goriely, *Astron. Astrophys.* **560** (2013) A128.

[11] S. Goriely, N. Chamel and J.M.Pearson, *Phys. Rev. C* **82** (2010) 035804.

[12] M. Baldo, G.F. Burgio, M. Centelles, B.K. Sharma and X. Viñas, *Phys. Atom. Nucl.* **77** (2014) 1157.

[13] M. Baldo, C. Maieron, P. Schuck and X. Viñas, *Nuc. Phys. A* **736** (2004) 241.

[14] G. Taranto, M. Baldo and G. F. Burgio, *Phys. Rev. C* **87** (2013) 045803.

[15] E. Garrido, P. Sarriguren, E. Moya de Guerra and P. Schuck *Phys. Rev. C* **60** (1999) 064312.

[16] M.N. Butler, D.W.L. Sprung and J. Martorell, *Nuc. Phys. A* **422** (1987) 157.

[17] G. Audi and A.H. Wasptra, *Nuc. Phys. A* **129** (2003) 337.

[18] I. Angeli, *At. Data Nucl. Data Tables* **87** (2004) 185.

[19] L.M. Robledo, M. Baldo and P. Schuck and X. Viñas, *Phys. Rev. C* **77** (2008) 051301; X. Viñas, L.M. Robledo, P. Schuck and M. Baldo, *Int. J. Mod. Phys. E* **18** (2009) 935; L.M. Robledo, M. Baldo and P. Schuck and X. Viñas, *Phys. Rev. C* **81** (2008) 034315.

[20] G. Baym, C.J. Pethick and P. Sutherland, *Astrophys. J.* **170** (1971) 299.

[21] X. Roca-Maza and J. Piekarewicz, *Phys. Rev. C* **70** (2008) 025807.

[22] J.M. Pearson, N. Chamel, S. Goriely and C. Ducoin, *Phys. Rev. C* **85** (2012) 065803.

[23] J. Antoniadis et al., *Science* **340** (2013) 1233232.